X-ray Absorption Spectroscopy Study of Solvation and Ion-Pairing in Aqueous Gallium Bromide Solutions at Supercritical Conditions

Cécile da Silva, Olivier Proux, Jean-Louis Hazemann, Julianne James-Smith, Denis Testemale, T. Yamaguchi

X-ray Absorption Spectroscopy Study of Solvation and Ion-Pairing in Aqueous Gallium Bromide Solutions at Supercritical Conditions

Cécile Da Silva[a], Olivier Proux[b], Jean-Louis Hazemann[a], Julianne James-Smith[a,c], Denis Testemale[a], Toshio Yamaguchi[d]

[a]Institut Néel, CNRS, Grenoble, France

[b]Laboratoire de Géophysique Interne et Tectonophysique, UMR CNRS/Université Joseph Fourier, Grenoble, France

[c]School of Earth and Environmental Sciences, University of Adelaide, South Australia

[d]Advanced Materials Institute and Department of Chemistry, Faculty of Science, Fukuoka University, Japan

olivier.proux@grenoble.cnrs.fr

Keywords: gallium bromide solution; ion solvation, ion pairing; supercritical fluids

Abstract

X-Ray Absorption Spectroscopy measurements have been performed both at the Ga and Br *K*-edges on aqueous $GaBr_3$ solutions. The isobaric experiments have been recorded at 30 MPa from ambient temperature to 670 K for two $GaBr_3$ concentrations (0.017 and 0.17 mol/dm^3). At room temperature, Ga^{3+} and Br^- ions are fully solvated, surrounded by water O atoms at 1.97 Å (Ga-O) and 3.37 Å (Br-O). When the temperature is elevated, Ga^{3+} cations precipitate as gallium oxy-hydroxide colloids while Br^- anions remain solvated. With a further increase in temperature, the gallium solid precipitates remarkably re-dissolved (25% and 50% for 0.017 and 0.17 mol/dm^3 respectively), due to the formation of $\left[GaBr_n(H_2O)_{4-n}\right]^{3-n}_{(aq)}$ (n=2, 3 or 4) tetrahedral complexes.

1. Introduction

Compared to water at ambient conditions, supercritical water (SCW) is unique in that it exhibits both gas-like and liquid-like properties. The high diffusivity and low viscosity of supercritical fluids enables them to penetrate and transport solutes from solid matrices. The smaller dielectric constant of SCW is responsible of the low solubility of inorganic salts. Since the solvation capacity of supercritical fluids depend on pressure and temperature, one can achieve the optimum conditions for a particular separation process by adjusting the temperature and pressure of the fluid phase, in decontamination process [1] or metal extraction [2] for example. By characterizing the ion-water (hydration), ion-ion (ion-pairing) and water-water (hydrogen bonding) interactions, the unique properties of such system can be inspected. However, these features remain in some cases unexplored because of experimental difficulties in structural and/or spectroscopic measurements at high temperatures and high pressures. One of the most appropriate techniques for the structural study of the local order around the ions in solution is the X-ray Absorption Spectroscopy (XAS) including both the x-ray-absorption near-edge structure (XANES) and Extended X-ray Absorption Fine Structure (EXAFS) spectroscopic techniques. This spectroscopy allows characterization of the local atomic environment around the absorbing element (selected from its absorption edge) to extract structural information on ions of interest. This is one reason why these techniques can be applied to dilute systems (several mM). These advantages also make it an ideal technique to study supercritical aqueous electrolyte solutions of low density in which the solubility of salts can be much lowered. Thus a High Pressure and High Temperature (*HP/HT*) cell dedicated to simultaneous fluorescence and transmission XAS measurements was developed and is now used routinely [3].

The behaviour with P and T of the bromide anion associated to monovalent [4-6] or

divalent cations [7-11] as counter ions in aqueous solutions is now well understood. The effect of ion-pairing in aqueous solutions, i.e. formation of pairs of oppositely charged ions with a common solvation shell, is a very rich topic. Ion-pair formations at high temperature and high pressure conditions, from an aqueous solution in which the ions are completely dissolved at ambient conditions, is mainly related to the strong decrease of the solvent permittivity with *T* [12]: it leads to the increase of the coulombic force between ions, a decrease of the solvation sphere and then ion pairing and formation of multi-ionic complexes. A limitation of the ion-pairing occurs close to the supercritical temperature and along the critical isochore: the onset of density fluctuations promotes the development of dense dynamic clusters of water molecules around the ions, leading to a screening effect which possibly inhibits the ion pairing processes [13]. Previous studies of MBr_2 (M = Mn [11], Ni [7], Zn [8-9]) aqueous solutions have clearly described this effect. An increase of the number of M-Br pairs associated to a dehydration phenomenon (drop of the number of O neighbours) is observed when increasing the temperature at a constant high pressure. Then, when reaching the supercritical conditions, M-Br and M-O distances decrease, while Br-O distances are invariant or tend to increase slightly.

In the present study we focus our effort on the trivalent cation, Ga^{3+}, with an ionic force superior than monovalent and divalent cations. Previous results from EXAFS, X-ray Diffraction and Raman experiments on the $GaBr_3$ system showed that the ion pairing effect occurred at ambient conditions in concentrated aqueous solutions ($[GaBr_3]$ =2.4 mol/dm^3) [14] and is not observed for concentrations lower than 1 mol/dm^3 [15]. The main aim of this experiment was to determine the evolution of the structure of the ionic hydration and/or pairing at various *P* and *T* in aqueous $GaBr_3$ solutions. XAS measurements have been performed simultaneously in fluorescence and transmission modes with the *HP/HT* cell, both at the Ga and Br *K*-edges. The isobaric experiments have been recorded at 30 MPa from

ambient temperature to 673 K for two $GaBr_3$ concentrations (0.017 and 0.17 mol/dm^3). The goal of this study is to probe the evolution of the local structure around Ga^{3+} and Br^- ions in solution, from ambient to supercritical state.

2. Experimental details

2.1. Sample preparation and the high pressure / high temperature device

Gallium bromide aqueous solutions were prepared by dissolving weighted amounts of $GaBr_3$ salts ($GaBr_3$, 99.999%, Sigma-Aldrich) in deionised water. The $GaBr_3$ solution concentrations are 0.017 and 0.17 mol/dm^3, with a measured pH equal to 2.7 and 1.9 respectively at ambient conditions. These concentrations are low enough in order to avoid any ion-pairing at ambient conditions [15].

The *HP/HT* cell used for these experiments has been described in details by Testemale *et al.* [3]. A schematic view of the set-up is shown in Fig. 1. The general principle consists of a helium-pressurized autoclave, and an internal sample container embedded in the heater. The main feature of the cell is then that the temperature and the pressure can be adjusted independently and are both stabilized by two independent pressure and temperature regulation devices [16]. For this particular study, the internal cell was in glassy carbon with a wall thickness machined down to 100 µm at the X-ray beam position, in order to limit the absorbance of the set-up as much as possible. The path length of the X-rays on the sample is 5 mm, the internal diameter of the carbon tube. Three apertures are present in the heater and vessel for the incident, transmitted and fluorescence beams. These apertures induce a small temperature difference between the value given by the thermocouple close to the furnace and the real sample temperature. A temperature calibration was then performed with pure water at 30 MPa, by determining the water density through X-ray absorption measurements. This is

done by precisely estimating the total X-ray absorption of all the constituents of the experimental system at 30 MPa: the two 0.8 mm beryllium windows of the vessel, the glassy carbon cell, the pressurized helium and the water at different furnace temperatures. The experimental estimation of the density of the water sample allows then to estimate the temperature of the sample area, by comparing to the theoretical density of water [17] and then to establish a temperature calibration curve. In the following, all the mentioned temperatures are the sample real temperature. The precision on the furnace temperature measurement equals to 0.1 K. Due to the uncertainty of the calibration curve, one can estimate the error bar on the sample temperature to ±2 K.

The following procedure was followed to run an isobaric experiment: the pressure was progressively applied with a constant slope of 1 MPa/min; when the pressure inside the cell reached 30 MPa, the target temperature was reached (with a slope of 10°/min), acquisitions were done (for each temperature, 3 spectra were acquired); then the temperature was increased to the next target temperature, and so on.

2.2. X-ray absorption measurements

X-ray absorption spectroscopy experiments were performed on the CRG-FAME beamline (BM30B), located at the European Synchrotron Radiation Facility storage ring in Grenoble, operating in 2*1/3 filling mode at 6 GeV. Spectra were recorded both in fluorescence and transmission modes (~40 min/scan data collection time), at the Ga and Br *K*-edges, using a double-crystal Si(220) monochromator [18]. The size, around 300x200 μm² (HxV, full width half maximum values), and the position of the X-ray spot on the sample were kept constant during the data acquisition. The full beam delivered by the bending magnet source was focused in the horizontal plane by the 2nd crystal of the monochromator and by the 2nd Rh-

coated mirror in the vertical plane. Finally, a feedback system was used to maximize the output of the two-crystal X-ray monochromator [19]. Acquisitions of the XAS spectra $\mu(E)$ were performed simultaneously in the transmission ($\mu_t(E).d = ln(I_0/I_t)$) and in the fluorescence modes ($\mu_f(E) \propto I_f/I_0$) where d is the thickness of the sample, I_0, I_t, I_f are the intensities of the incident, transmitted and fluorescence beams, respectively (see Fig. 1). Fluorescence detection was achieved using a 30 element energy-resolved detector.

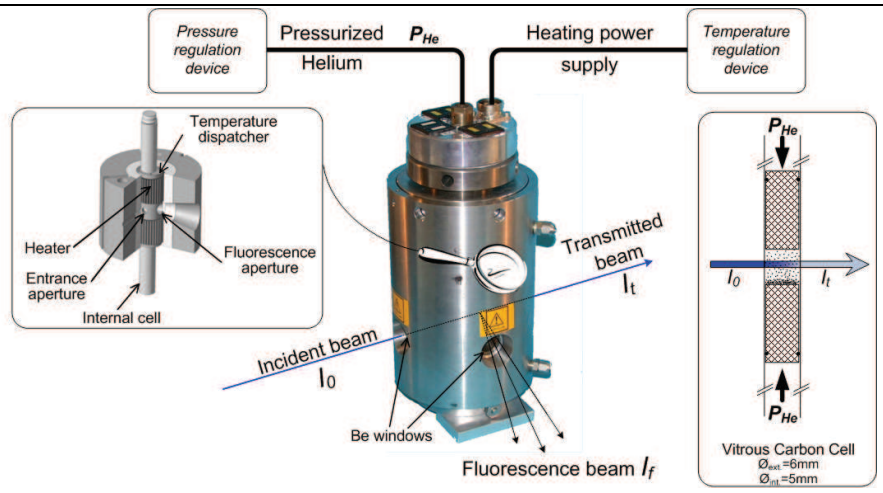

Fig. 1. Schematic view of the high pressure / high temperature vessel used for XAS measurements [3]. The gas pressure inside the vessel is stabilized with a special pressure regulation device [16]. Details of the internal heating system is shown in the left inset.

2.3. Extended X-ray Absorption Fine Structure analysis

A brief recall of the basic theory and fundamental analysis steps of EXAFS data treatment is present here. The spectra were reconstructed using the following formula [20], which describes the EXAFS oscillations within the framework of the cumulant expansion limited to the third order:

$$\chi(k)=S_0^2\sum_j N_j \frac{|f_j(k,\theta)|}{kR_j^2}\times e^{-2R_j/\lambda(k)}\times e^{-2k^2\sigma_j^2}\times \sin\left(\Phi_j(k)+2R_jk-\frac{4}{3}C_{3,j}k^3\right) \qquad (1)$$

The wavenumber k of the ejected photoelectron is given by $k = \sqrt{2m_e\left(E - E_{edge}\right)/\hbar^2}$, E_{edge} being the absorption edge energy. S_0^2 accounts for the central atom inelastic losses. The sum is taken over the j scattering paths (single or multiple scattering paths). N_j is the scattering path degeneracy (number of equivalent neighbors for single scattering). R_j is the half path length (central atom-neighbor distance for single scattering). $\left|f_j(k,\theta)\right|$ is the scattering amplitude experienced by the photoelectron while scattering from the neighbors ($\theta = \pi$ for backscattering). $\lambda(k)$ is the energy-dependent electron mean free path. $\Phi_j(k)$ is the phase shift due to the contributions both from the absorbing atom and the scattering atoms. The Debye-Waller factor, $e^{-2k^2\sigma_j^2}$ represents the mean-square variation of path length R_j, a measure of both static and dynamic disorder of path j, the anharmonicity of the pair distribution being expressed by the third cumulant $C_{3,j}$.

The XAS spectra at the Ga and Br *K*-edges were treated using the Horae package, comprising Athena and Artemis softwares [21]. XAS spectra were normalized to the absorption edge height (H), background-removed using the AUTOBK algorithm and weighted by k^2. Fourier filtration was done over the k range from ~ 2.5 to 12 Å^{-1} (depending on signal-to-noise ratio) using a Kaiser-Bessel apodization window to obtain the so-called radial distribution pseudo-function (RDF), which displays peaks roughly characteristic of each shell around the central atoms. Filtering of the RDF was done by inverse Fourier Transformation (FT) of the first peak(s) in the R-space.

$\left|f_j(k,\theta)\right|$, $\lambda(k)$ and $\Phi_j(k)$ were theoretically calculated using FEFF6.0 code [20]. The $\left|f_j(k,\theta)\right|$ backscattering amplitudes used for the calculations are gathered on Fig. 2. The backscattering amplitude of O atoms, both for the Ga or Br *K*-edge, has a maximum in the low k-region (around 4-5Å^{-1}) whereas the amplitude corresponding to heavier neighbours

such as Ga or Br is maximum in the medium *k*-region (around 8Å^{-1}). It is also important to mention that the Br-O-H-Br multiple scattering path has a really important amplitude, which represents approximately half of the Br-O-Br single scattering one. Simulations were performed on $k^2\chi(k)$ signals using either only single-scattering processes (Ga *K*-edge) or multiple-scattering ones (Br *K*-edge), to obtain the nature of the backscattering atoms, and for each single scattering path the coordination number (*N*), nearest-neighbor distance (*R*), its associated disorder term (σ^2) and if necessary the anharmonicity cumulant term C_3. In addition to these structural parameters, a parameter, ΔE, was varied to account for the difference between the experimental absorption-edge energy and its estimate made by FEFF.

The fitting procedure at the Ga *K*-edge was performed directly on the raw data. No anharmonicity cumulant term was used for the simulation, the total disorder being small enough to justify the description of the distribution function by a simple symmetric Gaussian function. It was also not necessary to take into account multiple scattering effects. The S_0^2 amplitude reduction factor was fitted to the EXAFS spectrum obtained at ambient temperature for the concentrated solution, with the number of O atoms on the first shell being known to be 6 [14-15].

Quantitative EXAFS analysis at the Br *K*-edge was performed on the filtered data at the Br *K*-edge, following the procedure described by Simonet *et al.* [8]. Complementary to the Br-O single-scattering paths, we added in the calculation the single- and multiple-scattering paths including the H atoms, *i.e.* Br-H, Br-H-O and Br-H-O-H paths to take into account the so-called focusing effect, which enhances the amplitude of the signals associated with linear configurations (Fig. 2b), [22]). The fact that the oxygen atoms are linked to the bromide via the hydrogen induces a disordered Br-O bond, and anharmonic treatments were then necessary to account for this disorder. Finally, the multi-electronic excitations were not taking into account, leading to tiny misfits between experiment and simulation around 5 and 7.5 Å^{-1}

[23]. The S_0^2 amplitude reduction factor was kept constant equal to unity during the optimisation procedure at this edge.

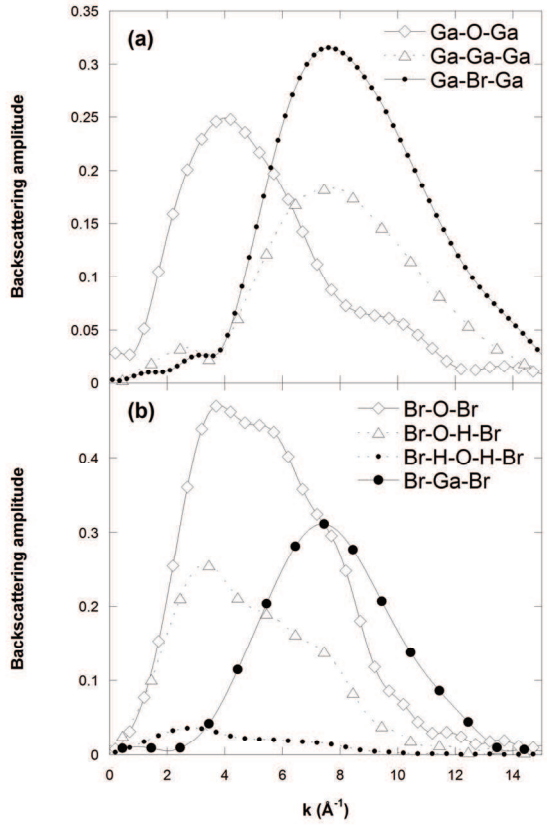

Fig. 2. Theoretical backscattering amplitude used for the simulations at the Ga (a) and the Br (b) *K*-edges: single scattering processes involving O, Ga or Br neighbour atoms around Ga and Br central atoms, and multiple scattering processes involving O and H atoms around Br central atoms. Calculations are performed with the FEFF6.0 code, with N=1 and σ^2=0.006Å^{-2}.

2.4. Concentration of the species in solution

The concentration $C(T)$ of the dissolved species at a given temperature (T) can be directly calculated from the absorption edge height $H_{trans.}(T)$ (see §2.3.) measured in the transmission mode [24]. This height is proportional to the density of the sample, the amount of dissolved absorbing species and the path length (l) of the X-ray beam inside the sample (constant, see right inset on Fig. 1):

$$H_{trans.}(T) \propto \rho(T) \times C(T) \times l \qquad (2)$$

where $\rho(T)$ is the density of the sample and $C(T)$ is the molality. The comparison of the $H_{trans.}(T)$ values provides information about composition changes in the fluid induced by the temperature increase. Salt precipitation produces for example a reduction of the edge heights larger than that expected from the fluid density evolution, because the solid precipitate falls out of the beam path. To precisely monitor the amount of ions or complexes which remain dissolved as a function of T, independently of the fluid density evolution and of the initial concentration, we calculate the relative concentration $C_R(T)$:

$$C_R(T) = \frac{C(T)}{C(300K)} = \frac{H_{trans.}(T)}{H_{trans.}(300K)} \times \frac{\rho(300K)}{\rho(T)} \quad (3)$$

For a simple calculation, we assume that the density of the sample is that of pure water, the influence of the concentration of the solvated species being rather small in the probed concentration range. Here we used the theoretical water density for $\rho(T)$ [17]. At room temperature, and for these rather low concentrations, all the Ga^{3+} and Br^- ions are dissolved. The relative concentration $C_R(T)$ is then directly the ratio of the dissolved quantity with respect to its total amount in the sample.

Errors on the $C_R(T)$ estimation are mainly due to the uncertainties on the height edge measurement and the temperature measurement for T>300 K. $\Delta C_R(T)$ can then be estimated simply from the differential form of equation 3:

$$\frac{\Delta C_R(T)}{C_R(T)} \approx \frac{\Delta H(T)}{H(T)} + \frac{\Delta H_{trans.}(300K)}{H_{trans.}(300K)} + \left|\frac{\delta\rho(T)}{\delta T}\right| \frac{\Delta T}{\rho(T)} \quad (4)$$

$\Delta H_{trans.}(T)$ is estimated to 0.001 and ΔT to 2 K (§2.1). From equation (4), it can be seen that the $\Delta C_R(T)$ error bar is maximum around the supercritical temperature where the decrease in the density is abrupt. $\Delta C_R(T)$ is around 0.6% at low temperature, around 3% in the supercritical region (the less favourable case). Moreover, these estimations are also slightly dependent on the initial assumption, i.e. the density of the sample is assumed to be that of

pure water, and the uncertainty might be higher than the 3% calculated with eq. 4. This is especially true close to the supercritical point of water where the misestimation of the density is the larger. One can then considered that the values obtained with eq. 3 allow a very good quantitative or semi-qualitative estimation of the real $C_R(T)$ evolution.

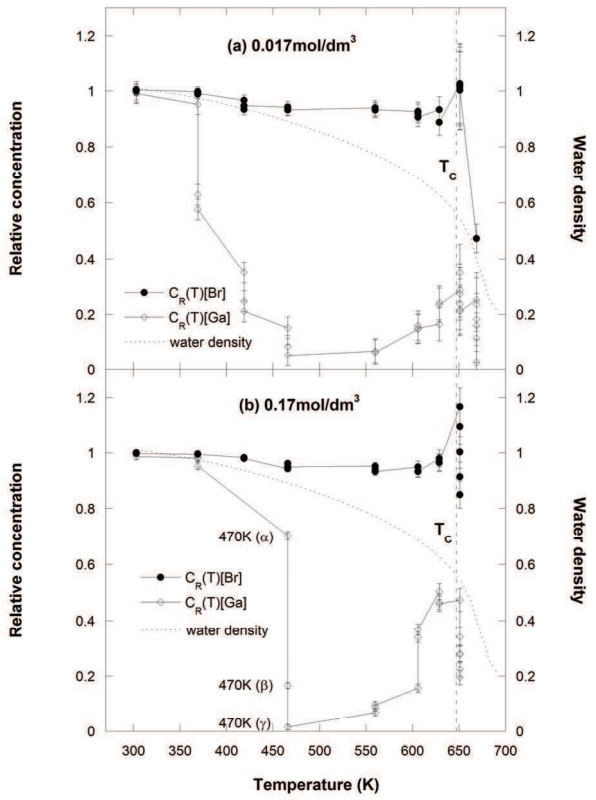

Fig. 3. Relative concentrations $C_R(T)$ of dissolved Ga and Br ions in water at 30 MPa as a function of the temperature. Measurements from the height of the absorption edge measured in the transmission mode both at the Ga and Br *K*-edges during EXAFS acquisitions (40 min. for each spectra). (a) $GaBr_3$ concentration 0.017 mol/dm^3. (b) $GaBr_3$ concentration 0.17 mol/dm^3. Comparison with the theoretical density of water [17].

3. Results

3.1. Qualitative analysis of the XAS spectra

The evolutions of the relative concentration $C_R(T)$ both for Ga and Br atoms are shown on Fig. 3. Normalized XANES spectra obtained at the Ga *K*-edge for the set of experiments

performed on the concentrated solution are gathered on Fig. 4. The $k^2.\chi(k)$ EXAFS spectra and the corresponding modulus of their Fourier Transform (FT) obtained are shown on Fig. 5 (Ga *K*-edge) and Fig. 6 (Br *K*-edge). For comparison, the spectra of reference model compounds are also shown: the spectrum of solid α-GaO(OH) obtained at the Ga *K*-edge by Pokrovski *et al.* [25] (Fig. 4 and Fig. 5) and that of the $GaBr_3$ salt (§2.1) measured at the Br *K*-edge in the transmission mode (Fig. 6). The structure of these compounds is known. α-GaO(OH) crystallizes in orthorhombic structure (space group P n m a [26]): Ga atoms are surrounded by 6 O atoms in the first shells forming a distorted octahedron and 8 Ga in the second shell. $GaBr_3$ salt structure is monoclinic (space group P 2_1/c [27]), built of Ga_2Br_6 molecules consisting of two $GaBr_4$ tetrahedra with a common Br-Br edge: 4 Br atoms are surrounded by one Ga atom (Br-Ga bond length: 2.26 Å) and 2 Br atoms by 2 Ga atoms (2.46 Å), i.e. the mean Br-Ga bond number equals to 4/3 with a mean bond length around 2.33 Å.

3.1.1. Concentration of ions in solution

The relative concentration of bromide in solution (Fig. 3) is stable around 1 for both sample solutions from 300 K to T_C (~647 K at 30 MPa) and then decrease to reach, at 670 K, ~0.4 (0.017 mol/dm^3) and ~0.8 (0.17 mol/dm^3).

The evolution of the gallium concentration with temperature (Fig. 3) is completely different. A sharp decrease occurs at 370 K (0.017 mol/dm^3) and 465 K (0.17 mol/dm^3), $C_R(T)$ reaching a value close to zero. The amount of gallium in solution is then estimated around 10^{-3} mol/dm^3 for both initial sample solutions. Then $C_R(T)$ increases slightly from 560 K, reaches a maximum close to 650 K before finally decreasing. This re-solvation of gallium reaches 25% and 50% of the total amount of gallium for 0.017 mol/dm^3 and 0.17 mol/dm^3 respectively.

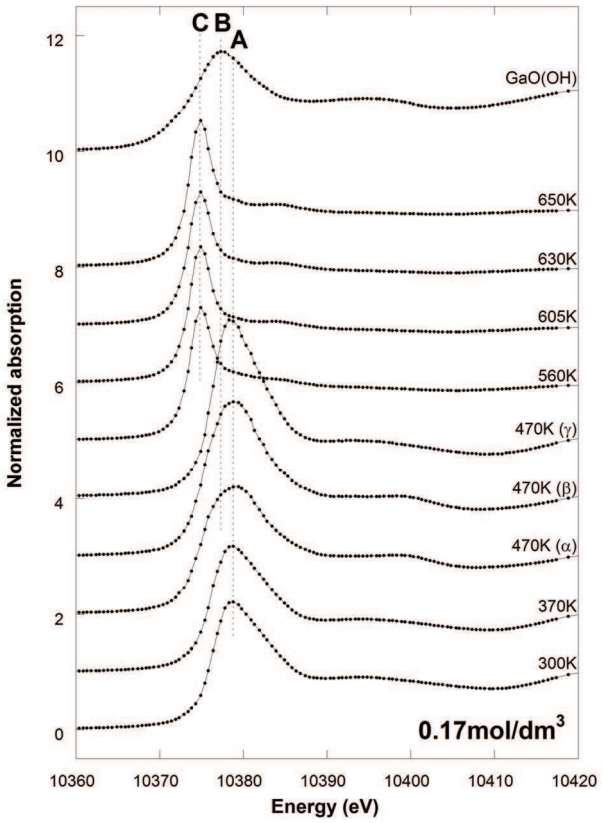

Fig. 4. Normalized XANES spectra obtained at the Ga *K*-edge for the 0.17 mol/dm^3 aqueous solution at 30 MPa and different temperatures. Comparison with the GaO(OH) spectra [25]. Spectra are shifted for clarity.

3.1.2. Ga cations solvation structure

Ga *K*-edge XANES spectra have been used as 'structural fingerprints' in order to determine the evolution of the gallium site geometry as a function of temperature. XANES spectra obtained for the concentrated solution at the Ga *K*-edge shows the presence of three different profiles (Fig. 4). At ambient conditions and at 370 K, the XANES displays an intense peak (the so-called white-line, labelled A) at 10379 eV and a large bump at higher energy (around 10394.5 eV). The intensity of the white line is related to the electronic transition probability $1s \rightarrow 4p$ and its position is assigned to octahedral species [28]. On the first spectrum at 470 K (α), a bump appears at 10399.5 eV, the width of the white line increases and its mean position shifts to higher energy. These features correspond to the characteristic features of the GaO(OH) spectrum, with a large white-line (B) at 10377.5 eV;

they are still clearly noticeable for the second spectrum at this temperature (β) but not for the last one (γ). For this last spectrum, the XANES seems similar to that of the octahedral species at 300 K and 370 K. At higher temperatures ($T \geq 560$ K) the feature at 10401 eV disappears and a thin white-line at 10375 eV is now clearly visible: such features have already been assigned to Ga tetrahedral environment [28].

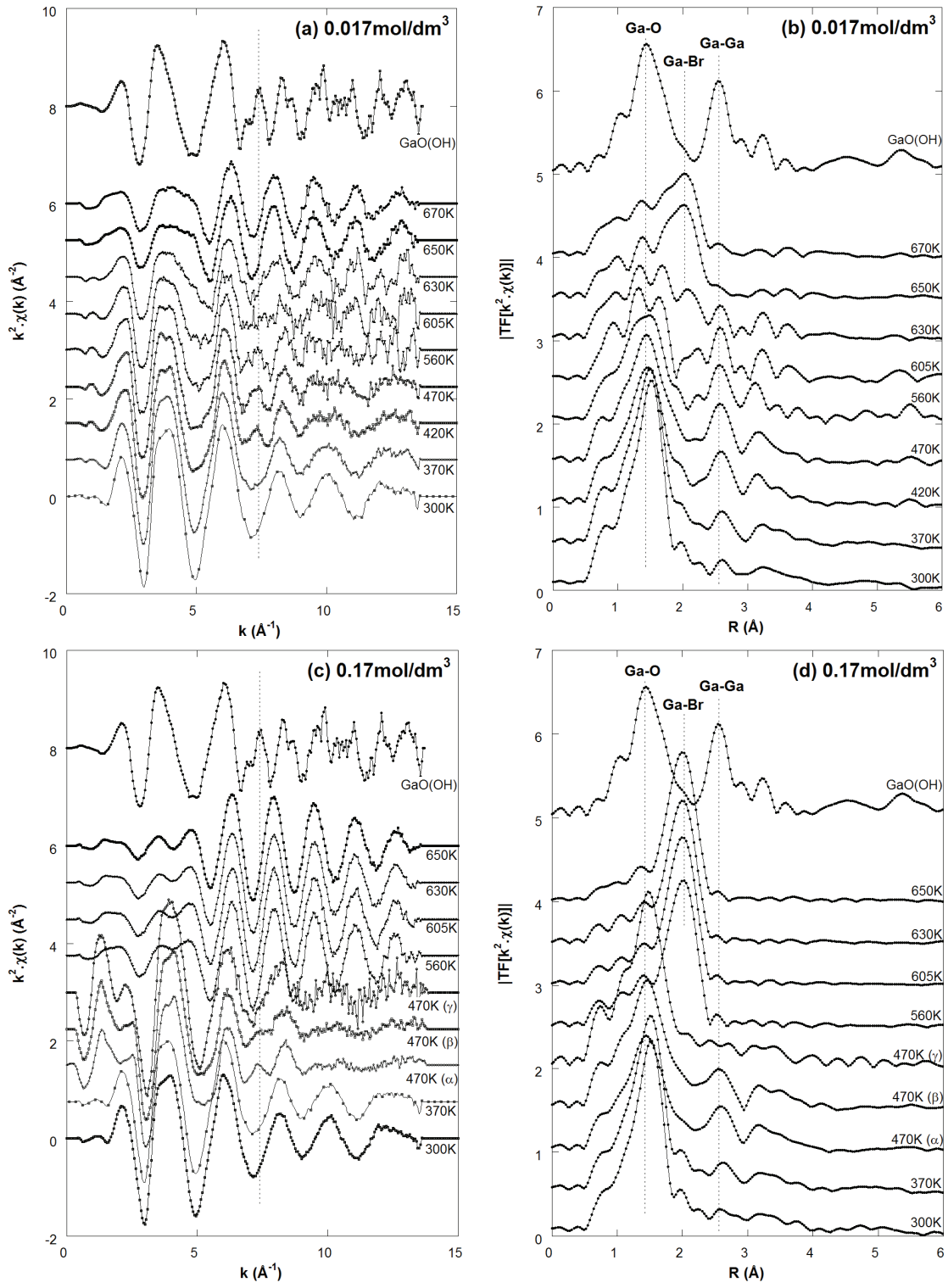

Fig. 5. EXAFS oscillations ($k^2.\chi(k)$, left figures, a and c) and modulus of their Fourier Transform (right figures, b and d) obtained for the $GaBr_3$ aqueous solution measured in the fluorescence mode at the Ga *K*-edge at 30 MPa at different temperatures for two concentrations, 0.017 mol/dm^3 (a and b) and 0.17 mol/dm^3 (c and d). Comparison with the GaO(OH) spectrum measured at ambient conditions in the transmission mode [25].

Complementary to this geometrical qualitative description of the gallium sites, the EXAFS spectra and their FT (Fig. 5) give quantitative information on the nature of the neighbours and structural parameters. Let us just recall that the backscattering amplitude of oxygen atoms, both for the Ga and Br *K*-edge, has a maximum in the low *k*-region (around 4-5 $Å^{-1}$) whereas backscattering of heavier atoms such as gallium or bromide is maximum in the medium *k*-region, around 8 $Å^{-1}$, (Fig. 2). At *T*=300 K, the $k^2.\chi(k)$ signal (Fig. 5a and 5c) is dominated in the low *k*-region by the oxygen backscattering. This contribution is clearly visible in the FT (Fig. 5b and 5d): a single peak centred around 1.4 Å constitutes the main part of the signal for both concentrations. At slightly higher temperatures ($T \geq 370$ K), another frequency appears in the oscillations, with beatings visible at 5 $Å^{-1}$ (*T*=420 K, the previous valley is less pronounced), 7.5 $Å^{-1}$ (clear appearance of a peak) and around 10 $Å^{-1}$ (the previous single oscillation in this *k*-range is now double). This evolution is clearly identifiable by comparing the FTs where a peak at 2.55 Å is more and more visible. All these features are in agreement with the EXAFS oscillations and FT of α-GaO(OH) solid reference, the second peak being associated to Ga-Ga bonds. For the diluted solution, this intermediate configuration seems to be stable from 370 K to 560 K (Fig. 5a and 5b). The three spectra performed at each temperature are perfectly superimposable and the magnitude of the features is roughly constant. At 630 K, this contribution to the total signal seems to have completely disappeared. On the other hand, for the concentrated solution (Fig. 5c and 5d), this structural feature is completely unstable. The first spectrum at 470 K (α) is rather similar to that of the diluted compound at the same temperature. The feature at 7.5 $Å^{-1}$ becomes smaller for the second one (β) and almost disappears for the third one (γ), the signal being then almost identical to the 300 K spectrum. On the FT (Fig. 5d), the peak at 2.55 Å is well defined for the two first spectra at 470 K (α and β) and vanishes completely for the third one (γ).

When the temperature increases to 650 K, the maximum of the envelope of the EXAFS

signal shifts to the high *k*-value and the contribution of the low *k*-region decreases (Fig. 5a and 5c). Such maximum of the amplitude of oscillations is compatible with the backscattering amplitudes of atoms heavier than oxygen, gallium or bromide (Fig. 2). This evolution is clearly seen on the FT (Fig. 5B and 5d) with the appearance of a peak centred around 2 Å. In the previous temperature range and by comparison with the α-GaO(OH) structure, the FT peak at 2.55 Å was attributed to Ga-Ga bonds. For these higher temperatures, the peak at 2 Å can then be attributed to Ga-Br ones. This evolution is progressive for $[GaBr_3]$=0.017 mol/dm^3. For $[GaBr_3]$=0.17 mol/dm^3 the structural modifications seem to be abrupt, the EXAFS signal being almost similar from 560 to 650 K.

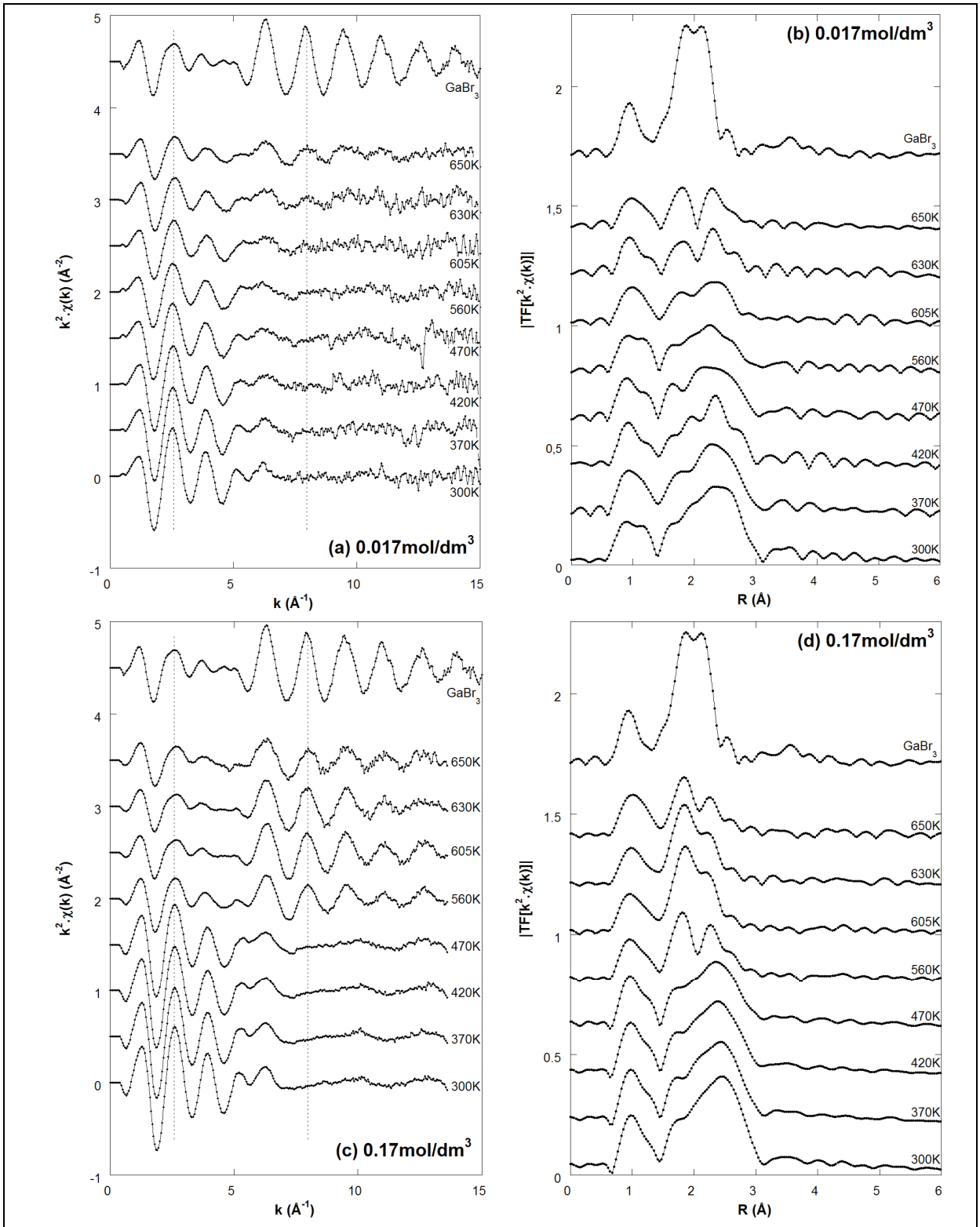

Fig. 6. EXAFS oscillations ($k^2.\chi(k)$, left figures, a and c) and modulus of their Fourier Transform (right figures, b and d) obtained for the $GaBr_3$ aqueous solution measured in the fluorescence mode at the Br *K*-edge at 30 MPa at different temperatures for two concentrations, 0.017 mol/dm^3 (a and b) and 0.17 mol/dm^3 (c and d).

3.1.3. Br anions solvation structure

Br *K*-edge XANES spectra (data not shown) are less informative than those obtained at the Ga *K*-edge. The spectra display a single large white line at a constant energy whatever the temperature of analysis. Reversely the $k^2.\chi(k)$ EXAFS spectra (Fig. 6a and 6c) and the FT functions (Fig. 6b and 6d) exhibit important changes with increasing temperature, for the two concentrations.

In the *k*-space, at ambient temperature, the signal is essentially dominated by the low *k*-region signal, characteristic of the Br-O backscattering (Fig. 2). No significant evolutions occur from 300 to 370 K. Between 370 and 560 K, a strong modification of the signal is clearly noticeable for the concentrated solution. The amplitude of the oscillations decreases in the low *k*-region until a contribution in the [6 - 13.5 $Å^{-1}$] *k*-range appears at 560 K which corresponds to the main oscillation of the $GaBr_3$ salt reference spectra, characteristic of Br-Ga bonds. This new contribution is also noticeable but with a smaller amplitude for the diluted solution. Moreover, concerning the $GaBr_3$ reference the $k^2.\chi(k)$ signal is dominated by this Br-Ga contribution, but the relative importance of the low *k*-region signal due to Br-O bonds shows that this salt reference might be slightly hydrated.

Important structural changes around Br atoms with increasing temperature are observed from the $k^2.\chi(k)$ spectra: these signatures are more subtle on the FT signal in the *R*-space (Fig. 6b and 6d). In a first temperature range ($T \leq 605$ K for the diluted solution, Fig. 6b, $T \leq 470$ K for the concentrated solution, Fig. 6d), the signal is dominated by a broad peak (from 1.45 to 3.15 Å, centred at 2.45 Å). This peak is attributed from the *k*-space analysis to Br-O bonds. For both solution at higher temperatures, the interference between the Br-O and Br-Ga contributions leads to a decrease of the FT peak modulus around 2 Å, in the middle of the peak. This destructive interference is also present for the $GaBr_3$ FT signal. Such a feature has already been observed for the $ZnBr_2$ system [9].

3.2. Quantitative analysis

Simulations were performed on merged spectra obtained at a given temperature and constant pressure. Before merging, we carefully checked the superimposition of these spectra, characteristic of a stability of the local structure around the probed element during the total acquisition time (around 2 hours for 3 spectra). Such a merging was possible for most of temperatures, even in some particular cases where the relative amount of the probed element slightly decreases (Fig. 3). At 470 K for the concentrated solution at the Ga *K*-edge, the EXAFS spectra are different and characteristic of evolving structures in solution. The spectra cannot be merged and the simulation is performed only on the last acquisition (labelled γ) where the amount of gallium is constant, at the experiment time scale, during all the acquisition.

Three different kinds of neighbours were necessary for the simulations: Ga-O and Br-O bonds characteristic of the hydration shell, Ga-Br and Br-Ga bonds characteristic of the ion-pairing, and Ga-Ga bonds. All the details of the simulations are given in Table 1 for the Ga *K*-edge and Table 2 for the Br *K*-edge. The number and distance of the first coordination shell (hydration and ion-pairing) simulations are also shown in Fig. 7 (Ga *K*-edge) and Fig. 8 (Br *K*-edge) and those concerning the Ga-Ga 2nd shell are gathered in Fig. 9 and Table 2. For comparison, the literature values obtained for the α- GaO(OH) structure in the literature are given in Table 1 [25], the values obtained in our study for the $GaBr_3$ salt at the Br *K*-edge in Table 2. Concerning this reference, Br atoms are surrounded by 1.05±0.1 Ga atoms, instead of 4/3 Ga atoms, at 2.33 Å, bond length in complete accordance with the mean value deduced from the structure of the $GaBr_3$ anhydrous salt [27]. Br atoms are also surrounded by 0.35±0.05 O atoms at 3.55 Å. These results are then characteristic of a slightly hydrated structure of the $GaBr_3$ salt with respect to the anhydrous one [27].

		O			Ga / Br			
Conc.	T	N_{Ga-O}	R_{Ga-O}	$\sigma^2_{Ga-O}\times10^3$	N_{Ga-X}	R_{Ga-X}	$\sigma^2_{Ga-X}\times10^3$	R
0.017 mol/dm^3	300	6.5 (0.9)	1.96 (0.01)	4.9 (1.8)				0.05
	370	6.6 (1.1)	1.97 (0.01)	6.3 (0.8)	*Ga*: 2.3 (0.7)	3.04 (0.05)	14 (7)	0.05
	420	6 6 (1.2)	1.94 (0.02)	11 (3)	*Ga*: 4.9 (0.8)	3.03 (0.05)	14 (7)	0.06
	470	6.9 (1.2)	1.94 (0.02)	13 (3)	*Ga*: 4.9 (0.8)	3.01 (0.04)	13 (6)	0.07
	560	6.3 (1.2)	1.93 (0.02)	13 (2)	*Ga*: 3.9 (0.8)	3.02 (0.02)	10 (2)	0.09
	605	5.4 (1.2)	1.92 (0.03)	16 (6)	*Ga*: 2.3 (0.7)	2.96 (0.02)	11 (2)	0.14
					Br: 0.4 (0.2)	2.31 (0.01)	4 (4)	
	630	4.6 (1.2)	1.90 (0.03)	19 (7)	*Ga*: 1.6 (0.7)	2.94 (0.02)	11 (2)	0.12
					Br: 1.4 (0.6)	2.31 (0.01)	5 (4)	
	650	3.0 (0.8)	1.89 (0.05)	18 (5)	*Br*: 2.8 (0.3)	2.32 (0.01)	7 (1)	0.03
	670	2.3 (0.5)	1.86 (0.03)	12 (4)	*Br*: 2.5 (0.3)	2.31 (0.01)	6 (1)	0.04
0.17 mol/dm^3	300	6 (fixed)	1.965 (0.01)	5.1 (0.6)				0.02
	370	5.6 (0.8)	1.97 (0.01)	5.2 (0.8)	*Ga*: 1.7 (0.6)	3.05 (0.04)	14 (5)	0.04
	470(γ)	6.6 (0.6)	1.97 (0.01)	8.3 (1.5)				0.04
	560	1.0 (0.3)	1.87 (0.02)	6.8 (0.4)	*Br*: 3.4 (0.2)	2.32 (0.01)	5.1 (0.4)	0.009
	605	0.6 (0.3)	1.86 (0.03)	6.0 (0.7)	*Br*: 3.6 (0.2)	2.32 (0.01)	5.7 (0.4)	0.009
	630	0.6 (0.3)	1.87 (0.03)	6.0 (0.6)	*Br*: 3.6 (0.2)	2.32 (0.01)	5.9 (0.4)	0.008
	650	0.3 (0.3)	1.90 (0.08)	6.0 (0.6)	*Br*: 3.8 (0.2)	2.32 (0.01)	6.1 (0.4)	0.012
α-GaO(OH) [25]		2.5 (0.5)	1.92 (0.01)	3.0 (0.5)	*Ga*: 2 (fixed)	2.95 (0.02)	4 (3)	
		3.0 (0.5)	2.05 (0.02)	3.0 (0.5)	*Ga*: 2 (fixed)	3.24 (0.02)	6 (3)	
					Ga: 4 (fixed)	3.41 (0.02)	9 (3)	

Table 1: Ga *K*-edge EXAFS analysis for the $GaBr_3$ solution at 30 MPa and increasing temperatures. Results for the first shell include Ga–O and Ga–Br pairs. Columns are successively related to concentration (mol/dm^3), temperature (K), number and nature of neighbours, pair distance (Å), σ^2 (Å^2, x10^3), energy shift ΔE (eV) and R factor characteristic of the goodness of the fit. S_0^2=0.892.

		O				Ga			
Conc.	T	N_{Br-O}	R_{Br-O}	$\sigma^2_{Br-O}\times10^3$	$C_3\times10^4$	N_{Br-Ga}	R_{Br-Ga}	$\sigma^2_{Br-Ga}\times10^3$	R
0.017 mol/dm^3	300	7.8 (0.8)	3.35 (0.05)	32 (3)	28 (19)				0.011
	370	6.2 (0.8)	3.44 (0.05)	31(4)	77(21)				0.013
	420	5.8 (1.6)	3.41 (0.09)	33(8)	68(42)				0.039
	470	5.6 (0.9)	3.46 (0.07)	36(6)	91(39)				0.022
	560	5.3 (0.9)	3.41 (0.08)	40(6)	84(37)				0.016
	605	3.4 (1.4)	3.35 (0.14)	31(10)	58(46)				0.08
	630	3.6 (1.3)	3.40 (0.1)	34(12)	89(19)	0.13(0.1)	2.32(0.03)	5(3)	0.03
	650	2.6 (0.9)	3.40 (0.1)	47(18)	106(50)	0.3(0.1)	2.31(0.01)	6(3)	0.023
0.17 mol/dm^3	300	8.3 (0.9)	3.37 (0.05)	30 (4)	37 (23)				0.014
	370	7.4 (0.9)	3.40 (0.06)	32 (5)	56 (26)				0.018
	420	6.9 (0.9)	3.40 (0.06)	34 (5)	62 (29)				0.018
	470	6.3 (0.9)	3.40 (0.07)	35 (6)	66 (34)				0.022
	560	6.5 (1.1)	3.40 (0.05)	53 (8)	83 (25)	0.7 (0.1)	2.30 (0.01)	7 (2)	0.008
	605	3.6 (1.0)	3.40 (0.05)	47 (13)	86 (23)	0.6 (0.2)	2.31(0.01)	7(1)	0.005
	630	3.6 (0.9)	3.40 (0.05)	36 (18)	112 (5)	1.0 (0.2)	2.31(0.01)	8(1)	0.015
	650	3.6 (1.5)	3.40 (0.05)	51 (15)	86 (23)	0.4 (0.1)	2.31(0.01)	5(1)	0.012
$GaBr_3$ salt		0.35 (0.05)	3.55 (0.05)	26 (15)	140 (20)	1.05 (0.1)	2.33(0.01)	4.5(5)	0.0005

Table 2: Br *K*-edge EXAFS analysis for the $GaBr_3$ solution at 30 MPa and increasing temperatures and for the $GaBr_3$ salt. Results for the first shell include Br–O and Br–Ga pairs. Columns are successively related to concentration (mol/dm^3), temperature (K), number and nature of neighbours, pair distance (Å), σ^2 (Å^2, x10^3), anharmonic C_3 term of the O shell (x10^4), energy shift ΔE (eV) and *R*-factor characteristic of the goodness of the fit. S_0^2=1.

3.2.1. EXAFS simulations of the first coordination shells

At ambient conditions at both concentrations, we find ~6 oxygen neighbours ($N_{Ga\text{-}O}$=6 by definition for the concentrated solution, §2.3) at 1.96 Å around Ga and ~8 at 3.36 Å around Br, in accordance with the literature [5,15,29]. For gallium (Fig. 7), the number of neighbours is also consistent with the octahedral site geometry found with the XANES analysis. When the temperature increases the number and bond length for Ga-O pairs are constant within uncertainty (T≤560 K) then decreases, to around $N_{Ga\text{-}O}$=2 (0.017 mol/dm^3) and 0.5 (0.17 mol/dm^3) and $R_{Ga\text{-}O}$=1.86-1.90 Å in the supercritical state (T≥605 K). Around Br (Fig. 8), the Br-O number continuously decreases to reach $N_{Br\text{-}O}$=2.6 (0.017 mol/dm^3) and 3.6 (0.17 mol/dm^3) with a $R_{Br\text{-}O}$ bond length equal to 3.40 Å as it was already found in other Br systems [3,7]. However such apparent strong dehydration process around the Br^- anions might be overestimated. Ferlat *et al.* have shown from EXAFS measurements associated with Molecular Dynamics simulations (MDEXAFS) a clear persistence of the Br^- hydration shell from normal to supercritical conditions [6]. The authors interpret this difference between the classical EXAFS analysis and the MDEXAFS one by the strong increase of the local disorder around the Br^- anion and not from a decrease of the number of neighbours. This strong disorder, due to dynamic local density fluctuations in addition to the classical bond length distribution, is well reproduced when one generates theoretical EXAFS spectra using snapshots of instantaneous configurations (MDEXAFS).

Close to T_C, simulations at the two K-edges give equivalent $R_{Ga\text{-}Br}$ and $R_{Br\text{-}Ga}$ bond lengths at 2.31-2.32 Å, a value slightly smaller than the value found in $[GaBr_4]^-$ measured in ambient conditions on concentrated solutions ($R_{Ga\text{-}Br}$=2.33-2.34 Å, [14]). At T=650 K for the concentrated solution, the total number of neighbours around gallium atoms is close to 4. For this temperature the number of Br bonded to Ga atoms is around N=2.8 (0.017 mol/dm^3) and 3.8 (0.17 mol/dm^3), much smaller than the number of Ga bonded to Br atoms, around 0.3-0.4 for the two concentrations at the same temperature.

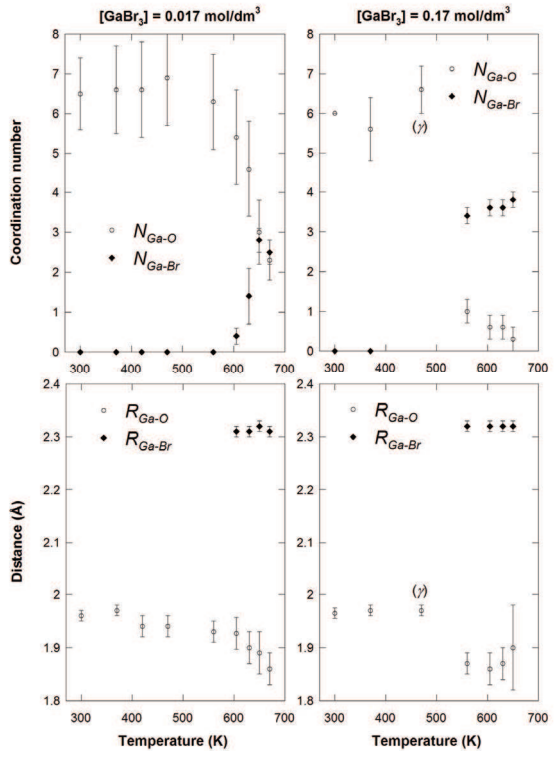

Fig. 7. Temperature evolution of the Ga-O and Ga-Br pair distances (bottom) and coordination numbers (top) at 30 MPa for the two studied concentrations, 0.017 mol/dm^3 (left) and 0.17 mol/dm^3 (right).

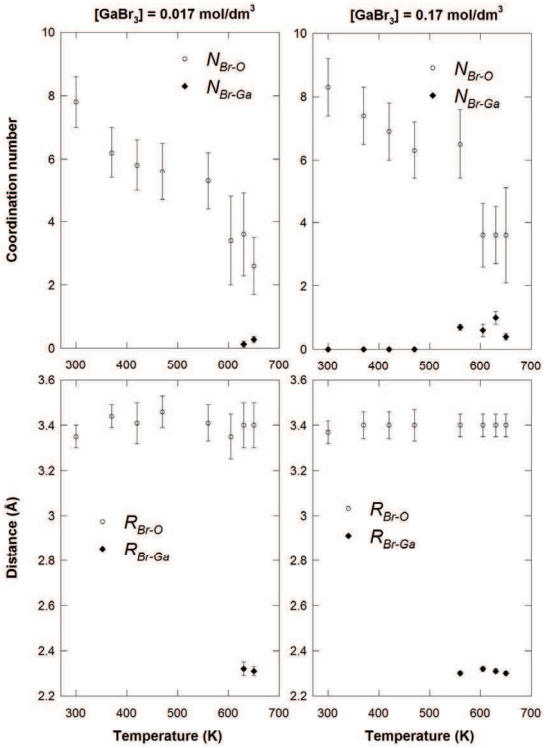

Fig. 8. Temperature evolution of the Br-O and Br-Ga pair distances (bottom) and coordination numbers (top) at 30 MPa for the two studied concentrations, 0.017 mol/dm^3 (left) and 0.17 mol/dm^3 (right).

3.2.2. EXAFS simulations of the second coordination shell around Ga atoms

The results of the EXAFS simulations for the second Ga-Ga coordination shell (Fig. 9), characteristic of the formation of a α-GaO(OH) like structure, are discussed only for the diluted solution due to the gallium precipitation occuring for the concentrated solution. The $N_{Ga\text{-}Ga}$ value, zero at 300 K, increases from 2.3 (370 K) to 4.9 (420 and 470 K). The value decreases then slightly in a first step (3.9 at 560 K), more strongly in a second one (2.3 at 605 K, 1.6 at 630 K). At 650 K no more Ga-Ga contribution is necessary for the simulation. The $R_{Ga\text{-}Ga}$ bond length value equal 3.04 Å at 370 K and decreases continuously to reach 2.94 Å at 630 K (Table 1, Fig. 9 bottom).

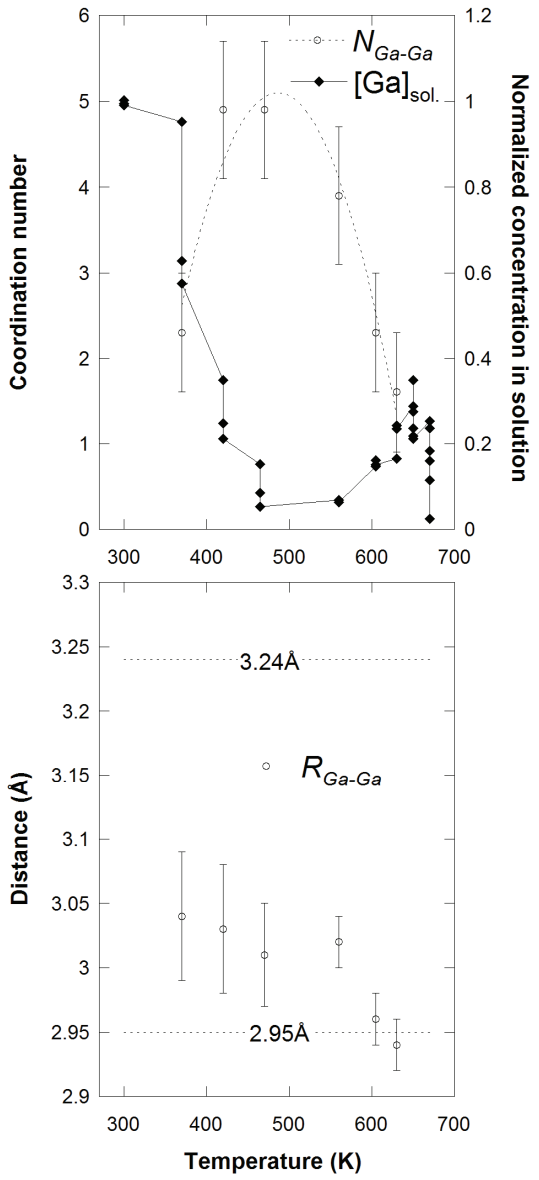

Fig. 9. Temperature evolution of the Ga-Ga pair distance (bottom) and coordination number (top) at 30 MPa. Comparison with the evolution of the relative concentration of Ga atoms in solution (top) and with the two first Ga-Ga bond lengths in GaO(OH) crystallized compound [25].

The presence of this Ga-Ga contribution can be directly correlated to the Ga concentration in solution (Fig. 9, top). The appearance of the Ga-Ga bonds at 370 K occurs simultaneously with the Ga precipitation. The N_{Ga-Ga} increases from 370 to 470 K while the ratio of gallium in solution is decreasing. At 605 K the decrease of N_{Ga-Ga} is associated with the increase of the amount of Ga in solution, which occurs simultaneously with the appearance of the Ga-Br

bonds (§ 3.2.1).

4. Discussion

4.1. Gallium oxy-hydroxide formation

The solubility and formation of α-GaOOH in aqueous solution has been extensively studied, both in basic and acid conditions [30,31]. In acid conditions, the following equilibrium occurs:

$$Ga^{3+}_{(aq)} + 2H_2O \leftrightarrow GaO(OH)\downarrow_{(s)} + 3H^{+}_{(aq)} \quad (5)$$

The reaction is endothermic [32]. Thus, the increase of temperature constitutes the driving force for such structural formation. In this study we probed only the Ga atoms which remained in solution (Fig. 1). The α-GaOOH solubility limit given in the literature [31] is low in these conditions, between 10^{-6} and 10^{-4} mol/dm^3 for pH ranging from 1.5 and 2.5 in the 423-523 K temperature range. These values are lower than the total amount of gallium estimated (10^{-3} mol/dm^3, §3.1.1). The structural state probed in our case is then far from equilibrium, the kinetic evolution being very low. Bénézeth *et al.* notice that the concentration limit is reached after typically one month, a time scale much more large than during our different sets of in situ experiment (the total counting time was around 40 minutes for each spectrum).

The mean Ga-Ga bond length is very close to the shorter distance of the crystallized α-GaO(OH) (Fig. 9, bottom), especially at high temperature. The local order in these crystallites or colloids in suspension is then surprisingly limited to the first shells around the central Ga atoms. Moreover, the $\sigma^2_{Ga\text{-}Ga}$ value associated to this bond is found really larger in the solution ($11\text{x}10^{-3}$ Å^2, at T=630 K) than in the solid reference ($4\text{x}10^{3}$ Å^2). In our experiments, $GaO(OH)_{(s)}$ formation takes place in disorder colloids or nano-crystallites in suspension,

followed by a precipitation.

4.2. Gallium-bromide ion pairing

At ambient conditions, Ga cations are entirely hydrated and octahedrally coordinated. At high temperature, Ga-Br association is clearly observed. The Ga-Br ion-pairing formation observed when the temperature increases is mainly driven by the evolution of Coulomb forces between ions. Indeed, the permittivity of water strongly decreases in high temperature conditions [12], and thus favours the attractive interaction between Ga cations and Br anions (the so-called ion pairing effect) by reducing the screening effect of the solvent. This effect has been detailed by Simonet et al. [9] for aqueous $ZnBr_2$ solution, for example. At T=650 K, Ga cations are surrounded by ~4 Br anions (3.8±0.2) in the 0.17 mol/dm^3 concentrated solution suggesting the presence of $[GaBr_4]^-$ complex. This EXAFS result is in accordance with the XANES spectrum obtained at this temperature for which the Ga cation was found in a tetrahedral site. Such a structure has been already determined by EXAFS and Raman spectroscopies on 1~2 mol/dm^3 $GaBr_3$ concentrated solutions at ambient conditions [14] but also with the trivalent analogous system $InCl_3$ in supercritical conditions where $[InCl_4]^-$ clusters are also formed [33]. If all the Ga atoms in solution formed $[GaBr_4]^-$ complex, the number of Ga-Br bonds, $N_{Ga\text{-}Br}$, deduced from the EXAFS measurement, would be 4. One can thus estimate the fraction of Ga cations in solution involved in such a structure from the ratio between the number of Ga-Br bonds measured in the solution (gathered in Table 2) and the Ga-Br bonds in the complete $[GaBr_4]^-$ structure (i.e., 4):

$$[\mathrm{Ga}]_{[\mathrm{GaBr_4}]^-} = \frac{N_{Ga-Br}}{(N_{Ga-Br})_{[\mathrm{GaBr_4}]^-}} = \frac{N_{Ga-Br}}{4} \quad (6)$$

It results that in the concentrated solution, almost all the Ga cations (95%) in solution

(which corresponds to ~50% of the total amount of Ga in the supercritical region, Fig. 3b) are linked to Br atoms in the $[GaBr_4]^-$ complex formation. On the other hand, the ratio of Br^- anions involved in ion-pairing remains small: each Br atoms presents less than one Ga neighbour (the theoretical value in the $[GaBr_4]^-$ structure) whereas the number of Br-O bonds remains high.

For the 0.017 mol/dm^3 solution in supercritical state, Ga^{3+} cations are simultaneously surrounded by similar numbers of Br^- anions and water molecules. This situation can be obtained in the case either of two different speciations for these cations ($[GaBr_4]^-$ complexes and hydrated Ga) or mixed species ($\left[GaBr_l(H_2O)_n^m\right]$). The second hypothesis is the most reasonable since one would expect progressive replacement of water molecules by bromide ions in the solvation shell of Ga^{3+} cations; the coexistence of the most brominated species along with the fully hydrated species seems doubtful. Literature results give ground to the existence of mixed species: in concentrated $GaBr_3$ solutions at ambient conditions $[GaBr_n(H_2O)_{4-n}]^{3-n}_{(aq)}$ (n=2 and 3) tetrahedral complexes are reported [14]. In high temperature hydrothermal $InCl_3$ solutions, binuclear indium chloride ($[In_2Cl(OH)]^{4+}$) was also observed [33]: however such analogous polynuclear complexes are not present in the present case since no Ga-Ga bonds were measured in supercritical conditions.

4.3. Comparison with other systems

Table 3 compares different systems probed by XAS where monovalent, divalent or trivalent cations are in aqueous solution with a halide anion (Br^- or Cl^-). We limit the comparison to the studies in which the initial concentration of salts in solution is low enough to avoid significant ion-pairing at ambient conditions. Ion pairing has not been observed for monovalent systems, even if molecular dynamic simulations predict a significant amount of

such pairing in supercritical conditions [5,34]. Ion pairing occurs for all these divalent or trivalent systems. Except for the two rare earth elements (Gd and Yb), ion pairing occurs in a tetrahedral form, in a mixed environment ($ZnCl_2(H_2O)_2$, $ZnBr_2(H_2O)_2$, $In_2Cl(OH)^{4+}$...) or pure form ($ZnCl_4^{2-}$, $ZnBr_4^{2-}$, $InCl_4^-$...). This structural form is consistent with the total number of neighbours around gallium cations found close to 4 in supercritical state. Ab initio simulations of the X-ray-Absorption Near Edge Structure (XANES) spectra measured during the EXAFS acquisitions are under progress to validate this geometry.

ions	reference	ion-pairing in supercritical conditions
Li^+, Cl^-	[35]	no ion pairing up to supercritical conditions ((LiCl]=3 and 9M)
Ag^+, Cl^-	[36]	no ion pairing up to 300°C and saturated vapour pressure ([$AgClO_4$]=0.1M, [$HClO_4$]=3M)
K^+, Br^-	[34]	simulations show the formation of a significant amount of ion-pairs in SC conditions[3,28], but EXAFS experiments do not allowed a validation of this point
Rb^+, Br^-	[4-6, 34]	
Cs^+, Br^-	[34]	
Ca^{2+}, Cl^-	[37]	ion pairing for [$CaCl_2$]=1M
Zn^{2+}, Cl^-	[38]	$ZnCl_2(H_2O)_2$ compound ([$ZnCl_2$]=2M) $ZnCl_4^{2-}$ compound ([$ZnCl_2$]=1M with an excess of Cl)
Sr^{2+}, Cl^-	[39]	no ion pairing up to 300°C and saturated vapour pressure ([$SrCl_2$]=0.1M, [HCl]=3M)
Mn^{2+}, Br^-	[11]	$MnBr_2(H_2O)_2$ compound ([$MnBr_2$]<1M) $MnBr_{2+n}(H_2O)_{2-n}$ compound ([$MnBr_2$]<1M with an excess of Br)
Ni^{2+}, Br^-	[7]	$NiBr(H_2O)_3$ compound ([$NiBr_2$]=0.2M) $NiBr_3(H_2O)$ compound ([$NiBr_2$]=0.2M+ [NaBr]=0.8M)
Zn^{2+}, Br^-	[8,9] [10]	$ZnBr_2(H_2O)_2$ compound for [$ZnBr_2$]=1M $ZnBr_4^{2-}$ compound for an excess of Br: [$ZnBr_2$]=1M + [NaBr]=6M
In^{3+}, Cl^-	[31]	$InCl_4^-$, $In_2Cl(OH)^{4+}$ compounds
Gd^{3+}, Cl^-	[40]	$GdCl_n(H_2O)_{7-n}^{+3-n}$ compound ([$GdCl_3$]=6mM with an excess of Cl)
Yb^{3+}, Cl^-	[41]	$YbCl_n(H_2O)_{7-n}^{+3-n}$ compound ([$YbCl_3$]=6mM with an excess of Cl)
Ga^{3+}, Br^-	this study	$GaBr_4^-$ ([$GaBr_3$]=0.17M), $Ga(H_2O)_{4-n}Br_n^{3-n}$ (n=2 or 3, [$GaBr_3$]=0.017M) compounds

Table 3: Ion pairing in aqueous solutions at supercritical conditions, M=mol/dm^3.

The predominant species in the supercritical state progressively evolve from mixed to pure solvation shell with a progressive dehydration when the relative concentration of halide anion increases. From our results there is however particularities for the $GaBr_3$ aqueous solution at the supercritical state. The Ga-Br association occurs in supercritical domain starting not from a situation where both the cation and the anion are hydrated but with the cation involved in an oxy-hydroxyde structure:

$$GaO(OH)_{(s)} + nBr^-_{(aq)} + 3H^+ \leftrightarrow \left[GaBr_n(H_2O)_{4-n}\right]^{3-n}_{(aq)} + (4-n)H_2O \qquad (7)$$

with n=2, 3 or 4. From these equilibrium equations, the relative concentration of Br^- anions with respect to the Ga^{3+} cations appears to be the key point to determine the main $[GaBr_n(H_2O)_{4-n}]^{3-n}_{(aq)}$ species in solution. This does not seem to be completely the case in our experiment: the initial [Br]/[Ga] ratio is always equal to 3 in both cases but we find a n value equal to 4 for the 0.17 mol/dm^3 solution and lower for 0.017 mol/dm^3. Moreover for both experiments 1) most of the Br^- anions are not involved in this association process, with the number of Br-O bonds being much higher than the Br-Ga ones at all the temperatures and 2) the main part of the Ga cations remain in the oxy-hydroxide form.

One possible explanation for this difference with other systems (see Table 3) may be found in the precipitation of $GaO(OH)_{(s)}$ that we observe in our experiments. Such oxy-hydroxide precipitation, and then dissolution, modifies strongly the pH conditions in the solutions. In both concentrated and diluted solutions, Ga concentration after precipitation of $GaO(OH)_{(s)}$ is similar (see Fig. 3), although Ga concentration was ten times higher in the 0.17 mol/dm^{3}solution: this indicates that more $GaO(OH)_{(s)}$ has been precipitated from the solution and the release of H^+ ions (see eq. 5), correlated to this precipitation, has been higher. This difference would increase the pH difference between the two solutions (the initial concentrated solution pH was smaller than the diluted one). Further investigations are necessary to determine precisely this equilibrium process and the influence of the acidity.

5. Conclusion

The local environment around Ga and Br atoms of $GaBr_3$ aqueous solution from ambient to supercritical state has been measured using XAS spectroscopy. At room temperature, Ga^{3+} and Br^- ions are fully solvated, surrounded by water O atoms at 1.97 Å (Ga-O) and 3.37 Å (Br-O). When the temperature increases, Ga^{3+} cations precipitate as $GaO(OH)_{(s)}$ in the

temperature range over 370 - 600 K, while Br^- ions remain completely solvated. For higher temperatures, Ga^{3+} cations are remarkably re-dissolved (25% and 50% for 0.017 and 0.17 mol/dm^3 respectively), ion-pairing occurs and pure or mixture tetrahedral specie $\left[GaBr_n(H_2O)_{4-n}\right]^{3-n}_{(aq)}$ (n=2, 3 or 4) complexes are formed ($R_{Ga\text{-}Br}$=$R_{Br\text{-}Ga}$=~2.31 Å). In supercritical conditions, an equilibrium occurs between $GaO(OH)_{(s)}$, Ga-Br-H_2O complexes and Br$^-$ anions which remain hydrated. Further investigations are necessary to determine precisely this equilibrium process.

Acknowledgements

The authors thank G. S. Pokrovski for providing the α-GaOOH reference spectrum and for fruitful discussions, E. Lahera, R. Bruyère and A. Prat for their great work on the *HP/HT* cell preparation and high pressure regulation system.

References

[1] G. Anitescu , L.L. Tavlarides, J. Supercrit. Fluids 38 (2006) 167–180.

[2] C. Erkey, J. Supercrit. Fluids 17 (2000) 259–287.

[3] D. Testemale, R. Argoud, O. Geaymond, J.-L. Hazemann, Rev. Sci. Instrum. 76 (2005) 043905.

[4] J. L. Fulton, D. M. Pfund, S. L. Wallen, M. Newville, E. A. Stern, Y. J. Ma, J. Chem. Phys. 105 (1996) 2161-2166.

[5] S. L. Wallen, B. J. Palmer, D. M. Pfund, J. L. Fulton, M. Newville, Y. J. Ma, E. A. Stern, J. Phys. Chem. A 101 (1997) 9632-9640.

[6] G. Ferlat, A. San Miguel, J.-F. Jal, J.-C. Soetens, P. Bopp, I. Daniel, S. Guillot, J.-L. Hazemann, R. Argoud, Phys. Rev. B 63 (2001) 134202/1-9.

[7] M. M. Hoffmann, J. G. Darab, B. J. Palmer, J. L. Fulton, J. Phys. Chem. A 103 (1999) 8471-8482.

[8] V. Simonet, Y. Calzavara, J.-L. Hazemann, R. Argoud, O. Geaymond, D. Raoux, J. Chem. Phys. 116 (2002) 2997-3006.

[9] V. Simonet, Y. Calzavara, J.-L. Hazemann, R. Argoud, O. Geaymond, D. Raoux, J. Chem. Phys. 117 (2002) 2771-2781.

[10] R. A. Mayanovic, A. J. Anderson, W. A. Bassett, I.-M. Chou, Chem. Phys. Lett. 336 (2001) 212-218.

[11] Y. Chen, J. L. Fulton, W. Partenheimer, J. Am. Chem. Soc. 127 (2005) 14085-14093.

[12] Y. Guissani, B. Guillot, J. Chem. Phys. 98 (1993) 8221-8236.

[13] D. Testemale, M. V. Coulet, J.-L. Hazemann, J.-P. Simon, F. Bley, O. Geaymond, R. Argoud, J. Chem. Phys. 122 (2005) 194505.

[14] P. Smirnov, H. Wakita, M. Nomura T. Yamaguchi, J. Solution Chem. 33 (2004) 903-922.

[15] P. Lindqvist-Reis, A. Muñoz-Páez, S. Díaz-Moreno, S. Pattanaik, I. Persson, M.

Sandström, Inorg. Chem. 37 (1998) 6675-6683.

[16] R. Bruyère, A. Prat, C. Goujon, J.-L. Hazemann, J. Phys. Conf. Series (2008) to be published.

[17] E.W. Lemmon, M.O. McLinden, D.G. Friend, NIST Chemistry WebBook, NIST Standard Reference Database 69 (2005), Eds. P.J. Linstrom and W.G. Mallard, June 2005, National Institute of Standards and Technology, Gaithersburg MD, 20899 (http://webbook.nist.gov).

[18] O. Proux, X. Biquard, E. Lahera, J.-J. Menthonnex, A. Prat, O. Ulrich, Y. Soldo, P. Trévisson, G. Kapoujvan, G. Perroux, P. Taunier, D. Grand, P. Jeantet, M. Deleglise, J.-P. Roux, J.-L. Hazemann, Phys. Scripta 115 (2005) 970-973.

[19] O. Proux, V. Nassif, A. Prat, O. Ulrich, E. Lahera, X. Biquard J.-J., Menthonnex, J.-L. Hazemann, J. Synchrotron Rad. 13 (2006) 59-68.

[20] J. J. Rehr, R. C. Albers, Rev. Mod. Phys. 72 (2000) 621-654.

[21] B. Ravel, M. Newville, J. Synchrotron Rad. 12 (2005) 537–541.

[22] P. D'Angelo, N. V. Pavel, J. Synchrotron Rad. 8 (2001) 173-177.

[23] P. D'Angelo, A. Di Cicco, A. Philipponi, N. V. Pavel, Phys. Rev. A 47 (1993) 2055-2063.

[24] G. S. Pokrovski, J. Roux, J.-L. Hazemann, D. Testemale, Chem. Geol. 217 (2005) 127-145.

[25] G.S. Pokrovski, J. Schott, J.-L. Hazemann, F. Farges, O.S. Pokrovsky, Geochim. Cosmochim. Acta 66 (2002) 4203-4222.

[26] S. Li, C. Zheng, K.C. Lobring, Zeit. Kristallog. 218 (2003) 11-12.

[27] S. I. Troyanov, T. Krahl, E. Kemnitz, Zeit. Kristallog. 219 (2004) 88-92.

[28] K. Nishi, K. Shimizu, M. Takamatsu, H. Yoshida, A. Satsuma, T. Tanaka, S. Yoshida, T. Hattori, J. Phys. Chem. B 102 (1998) 10190-10195.

[29] O.S. Pokrovsky, G.S. Pokrovski, J. Schott, J. Colloid Interface Sci. 279 (2004) 314-325.

[30] I.I. Diakonov, G.S. Pokrovski, P. Benezeth, J, Schott, J.-L. Dandurand, J. Escalier, Geochim. Cosmochim. Acta 61 (1997) 1333-1343.

[31] P. Benezeth, I.I Diakonov., G.S. Pokrovski, J.-L. Dandurand, J. Schott, I.L. Khodakovsky, Geochim. Cosmochim. Acta 61 (1997) 1345-1357.

[32] H. R.Craig, S. Y. Tyree, Inorg. Chem. 8 (1969) 591-594.

[33] T. M. Seward, C.M.B. Henderson, J.M. Charnock, Chem. Geol. 167 (2000) 117–127.

[34] G. Ferlat, A. San Miguel, J. F. Jal, J. C. Soetens, Ph. A. Bopp, J. L. Hazemann, D. Testemale, I. Daniel, J. Mol. Liq. 101 (2002) 127-136.

[35] T. Yamaguchi, A. K. Soper, J. Chem. Phys. 110 (1999) 3529-3535.

[36] T.M. Seward, C.M.B.Henderson, J.M. Charnock, B.R. Drobson, Geochim. Cosmochim. Acta 60 (1996) 2273-2282.

[37] J. L. Fulton, Y. Chen, S. M. Heald, M. Balasubramanian, J. Chem. Phys. 125 (2006) 094507.

[38] R. A. Mayanovic, A. J. Anderson, W. A. Bassett, I.-M. Chou, J. Synchrotron Radiat. 6 (1999) 195.

[39] T.M. Seward, C.M.B. Henderson, J.M. Charnock, T. Driesner, Geochim. Cosmochim. Acta 63 (1999) 2409-2418.

[40] R. A. Mayanovic, A. J. Anderson, W. A. Bassett, I.-M. Chou, Chem. Geol. 239 (2007) 266–283.

[41] R. A. Mayanovic, S. Jayanetti, A. J. Anderson, W. A. Bassett, I.-M. Chou, J. Phys. Chem. A 106 (2002) 6591-6599.